CrossMark

ORIGINAL PAPER

Photoreceptor projections and receptive fields in the dorsal rim area and main retina of the locust eye

Fabian Schmeling · Jennifer Tegtmeier ·
Michiyo Kinoshita · Uwe Homberg

Abstract In many insect species, photoreceptors of a small dorsal rim area of the eye are specialized for sensitivity to the oscillation plane of polarized skylight and, thus, serve a role in sky compass orientation. To further understand peripheral mechanisms of polarized-light processing in the optic lobe, we have studied the projections of photoreceptors and their receptive fields in the main eye and dorsal rim area of the desert locust, a model system for polarization vision analysis. In both eye regions, one photoreceptor per ommatidium, R7, has a long visual fiber projecting through the lamina to the medulla. Axonal fibers from R7 receptors of the dorsal rim area have short side branches throughout the depth of the dorsal lamina and maintain retinotopic projections to the dorsal medulla following the first optic chiasma. Receptive fields of dorsal rim photoreceptors are considerably larger (average acceptance angle 33°) than those of the main eye (average acceptance angle 2.04°) and, taken together, cover almost the entire sky. The data challenge previous reports of two long visual fibers per ommatidium in the main eye of the locust and provide data for future analysis of peripheral networks underlying polarization opponency in the locust brain.

Keywords Compound eye · Dorsal rim area · Receptive fields · Photoreceptor projections · Desert locust

F. Schmeling · J. Tegtmeier · U. Homberg (✉)
Faculty of Biology, Animal Physiology, Philipps University of Marburg, 35032 Marburg, Germany
e-mail: homberg@biologie.uni-marburg.de

M. Kinoshita
Laboratory of Neuroethology, Sokendai (The Graduate University for Advanced Studies), Shonan Village, Hayama, Kanagawa 240-0193, Japan

Introduction

The polarization pattern of the blue sky is one of several celestial cues that are used by insects as directional reference in sky compass orientation (reviewed in Horváth and Varjú 2004; Wehner and Labhart 2006; Homberg and el Jundi 2013). Navigational responses to polarized light have been documented in several insect species under field and laboratory conditions (honeybee: von Frisch 1949; field cricket: Brunner and Labhart 1987; flies: von Philipsborn and Labhart 1990; Weir and Dickinson 2012; dung beetle: Dacke et al. 2003; desert locust: Mappes and Homberg 2004; monarch butterfly: Reppert et al. 2004; desert ant: Wehner and Müller 2006), and in all species studied, orientation responses to dorsally presented polarized light are mediated by specialized photoreceptors in a dorsal rim area (DRA) of the compound eye.

Photoreceptors of the DRA involved in polarization plane signaling share a number of specializations across insect species (Labhart and Meyer 1999). High polarization sensitivity is achieved by highly aligned microvilli, organized in two orthogonally arranged blocks in each DRA ommatidium. Further specializations include homochromacy, i.e., identical spectral sensitivity of DRA photoreceptors that contribute to polarization vision in the UV (honeybee, desert ant), blue (field cricket, desert locust), or green (cockchafer) range of the spectrum. As demonstrated in crickets, high absolute sensitivity of DRA photoreceptors to polarized light is, finally, accomplished by the lack of screening pigment, resulting in considerably wider receptive fields than in photoreceptors of the main retina (Labhart et al. 1984).

In the desert locust, DRA ommatidia contain 8 photoreceptor cells with the microvilli of R7 orthogonally opposing those of the remaining cells R1-6 and R8 (Homberg

Springer

and Paech 2002). Opponent processing of signals from these two sets of photoreceptors is believed to underlie the phenomenon of polarization opponency (Labhart and Petzold 1993; Wehner and Labhart 2006), found widely in polarization-sensitive interneurons in the brains of crickets, locusts, and monarch butterflies (Homberg et al. 2011).

Following our analysis of opsin expression patterns and spectral sensitivities of photoreceptors of the DRA and main eye of the desert locust (Schmeling et al. 2014), we report here on the patterns of central axonal projections of photoreceptors and their receptive fields. The data complement our earlier investigation and provide an important basis for future analysis of peripheral mechanisms in polarized light processing in the desert locust and other insects.

Materials and methods

Animal rearing

Experiments were performed on gregarious and solitarious desert locusts (*Schistocerca gregaria*). Gregarious adult male and female locusts were obtained from breeding colonies at the University of Marburg. Animals were kept in crowded cultures at 12:12 h light:dark cycle, 28 °C room temperature, and 50 % relative humidity. Following the conditions established by Roessingh et al. (1993), solitarious male and female animals were reared individually in small boxes at 12:12 h light:dark cycle, at 26.5 °C and 60 % relative humidity. Care was taken to ensure that no visual, olfactory and mechanical contact occurred between individuals. Animals were reared in solitarious conditions for at least three generations before being used for experiments. For identifying the solitarious phase, typical morphological characteristics such as body coloration and size (Simpson et al. 1999; el Jundi and Homberg 2012) were observed. Only locusts at least one week after imaginal moult were used for experiments.

Electrophysiology and visual stimulation

Animal preparation, experimental setup, and procedures for intracellular recording were identical with those in Schmeling et al. (2014). To compare angular sensitivity data from different animals, great care was taken to position and orient locusts in the experimental setup in identical ways by microscopic inspection of the locust`s head in relation to visual landmarks of the perimeter apparatus. Intracellular recordings were obtained from DRA and non-DRA photoreceptor cells in the locust eye using glass microelectrodes. The electrode tips were filled with 4 % Neurobiotin (Vector Laboratories, Burlingame, UK) in 1 mol l^{-1} KCl backed up with 3 mol l^{-1} KCl. The resistance of the

electrodes in the tissue was 30–100 MΩ. Recording electrodes were inserted into the retina through a small hole cut into the cornea, while a silver wire serving as the indifferent electrode was inserted into the head capsule of the locust. Signals were amplified 10x. Digitized data were stored on a PC using Spike 2 or pClamp10 software with a sampling rate of 2 kHz.

For visual stimulation, a xenon arc lamp served as the light source. Wavelength and intensity of light produced by the xenon lamp could be modulated by a monochromator and a set of neutral density filters. The resulting light beam was focused to the end of a light guide. The other end of the light guide was pointed at the locust's eye. It was fixed to the arm of a perimeter and could be moved along a virtual sphere with the locust's head in its center (angular size at the eye 3°). Monochromator and neutral density filters were controlled by custom-made software.

After penetrating a photoreceptor cell, the light guide was positioned in the center of the receptor's receptive field determined as the position eliciting maximum responses to a series of light flashes. The spectral type of the photoreceptor was determined by testing a series of monochromatic light flashes of equal quantal flux (310–630 nm in 20 nm steps; stimulus duration 500 ms). Quantum flux was adjusted in each recording to elicit responses within the range of the intensity response curve. In some cases only 350, 450 or 530 nm were tested to roughly determine the spectral type.

Response–stimulus intensity (*V*-log *I*) functions were obtained by recording the responses to light flashes of the peak wavelength of the receptor, starting at low light levels, up to the maximum intensity (310–350 nm: 2.8×10^{13} photons cm^{-2} s^{-1}, 410–450 nm: 3.9×10^{13}, 510–530 nm: 2.8×10^{13}) of the setup. Light intensities were calibrated with a radiometer (P-9201, Gigahertz-Optic, Puchheim, Germany).

Angular sensitivity was measured using the wavelength eliciting the largest response by moving the light guide along the horizontal and vertical axis around the animal's head. When recording from the DRA, 5° or 10° steps were made between two light flashes. Step size was 1° when recording from the main retina, starting from the visual center. Subsequently, Neurobiotin was injected iontophoretically into the cell by constant depolarized current (0.5–2 nA for 1–3 min).

Data evaluation: electrophysiology

For angular sensitivity measurements, relative sensitivities at the tested positions were calculated by converting voltage amplitudes to equivalent photon numbers from the *V*-log *I* function of the receptor (see Schmeling et al. 2014). The normalized reciprocal of the relative photon number

was then calculated as the relative sensitivity. Sensitivity values were plotted as a function of angular stimulus position. Because the positions for sensitivity measurements along horizontal directions were not on a great circle around the locust`s head, their perimeter readings were corrected accordingly (Burkhardt and Streck 1965). Acceptance angles were determined as the half widths of the plotted functions at 50 % relative sensitivity. V-log I curve processing and graph plotting were performed with Origin6 software (Microcal Software, Northhampton, USA). SPSS software (version 19) was used for statistical evaluations. The Shapiro–Wilk test was used to test for normality of data distribution. Group testing of not normally distributed data was performed with the Kruskal–Wallis test.

Histological procedure for single cell staining

Tissue preparation and histological procedures were similar to those in Schmeling et al. (2014). Optic lobes were removed from the head capsule and immersed in Neurobiotin fixative (4 % paraformaldehyde, 0.25 % glutaraldehyde, 2 % saturated picric acid, in 0.1 mol l^{-1} phosphate buffer) at 4 °C. After rinsing in phosphate-buffered saline (PBS, 0.1 mol l^{-1}, pH 7.4) for 4 × 15 min and preincubation in normal goat serum (NGS, 5 % in PBS) for 3 h at room temperature, incubation with streptavidin-Cy3 conjugate (1:1000) for 2–3 days and primary antibody against *Drosophila* synapsin (1:30) in 0.1 mol l^{-1} PBS/0.3 % Triton X-100/1 % NGS followed. The monoclonal anti-synapsin antibody (SYNORF1, kindly provided by Dr. E. Buchner, Würzburg, Germany) was raised in mouse against fusion proteins consisting of glutathione-S-transferase and the *Drosophila* SYN1 protein (Klagges et al. 1996). It labels synaptic neuropil as demonstrated in several insect species (e.g., *Drosophila*: Klagges et al. 1996; *Schistocerca*: Heinze and Homberg 2008). After rinsing in 0.1 mol l^{-1} PBS + 0.3 % Triton X-100 for 4 × 15 min, incubation proceeded with a secondary antibody (0.8 % goat anti mouse-Cy5, 0.1 % streptavidin-Cy3 and 1 % NGS in 0.1 mol l^{-1} PBS + 0.3 % Triton X-100) at 4 °C for 2 days. The preparations were dehydrated in an ethanol series and embedded in soft Spurr's embedding medium (Spurr 1969). Sections were cut with a rotary microtome (Leitz, Wetzlar, Germany) in orientations with respect to the observed structure and were, finally, embedded in Permount (Fisher Scientific, Pittsburgh, PA, USA) under glass coverslips.

Mass staining of photoreceptors

Animals were immobilized by cutting off their legs and wings. Movable body parts were fixed with wax. For tracer injection into the optic lobe, the head capsule was opened frontally. Ocelli and antennae were removed, leaving the compound eyes and the central brain intact. A cut was made in the neurilemma in the region of either the dorsal rim of the medulla or the medulla. A single crystal of dextran conjugated to the fluorescent dye Texas Red (3,000 MW, Molecular Probes, Eugene, OR, USA) was inserted into the opening and was taken up by the damaged fibers.

For dye application to the DRA of the retina, small cuts were made into the cornea anteriorly and posteriorly in the DRA. Crystals of dextran–Texas Red were applied to the anterior and crystalline Neurobiotin to the posterior hole. For staining photoreceptors of the main retina, large parts of the retinal cornea were removed, and dextran–Texas Red was applied to the bare retina.

If dextran–Texas Red was solely applied, animals were left for about two hours at 4 °C in humid conditions to allow for diffusion of the tracer. Afterwards, brains were dissected from the head capsule and kept in fixative solution composed of 1 part 0.2 mol l^{-1} cacodylate and 1 part 4 % paraformaldehyde for another two hours. The optic lobes were then washed in 0.2 mol l^{-1} cacodylate for 10 min. When Neurobiotin and dextran–Texas Red were coapplied as tracers followed by synapsin immunostaining, brains were fixed in Neurobiotin fixative over night. Optic lobes were rinsed in 0.1 mol l^{-1} PBS containing 1 % Triton X-100. After preincubation in 5 % normal goat serum, primary antibody against *Drosophila* synapsin (1:30) (see Klagges et al. 1996) was applied in 0.1 mol l^{-1} PBS/0.3 % Triton X-100/1 % NGS. Incubation with secondary antibody (0.8 % goat anti mouse-Cy5) and 0.1 % streptavidin-Cy3 diluted with 1 % NGS in 0.1 mol l^{-1} PBS + 0.3 % Triton X-100 followed at 4 °C for 2 days. In all cases, optic lobes were dehydrated in an ascending ethanol series, transferred to propylene oxide and finally embedded in soft Spurr`s resin. Sections of 8–10 μm for retina tissue and 60 μm for optic lobe tissue were made with a rotary microtome in individual orientations. Starting from the incubation with fluorophores, the preparations were kept in the dark as much as possible.

Confocal microscopy

Stained sections were scanned with a confocal laser scanning microsope (TCS SP5, Leica Microsystems, Wetzlar, Germany), using a 10× objective (HC PL APO 10×/0.4 Imm Corr CS; Leica, Bensheim, Germany) for overviews and a 63× objective (HCX PL APO 63×/1.32 OIL PH 3CS; Leica) for details (scanning intervals 1–2 μm). A He/Ne laser (excitation wavelength 543 nm for Cy3 and 595 nm for Texas Red) and an Ar/Kr laser (excitation wavelength 647 nm for Cy5) were used to detect fluorescence. Image processing was performed with CLSM imaging software (LAS AF v. 2.2.1 build 4842, Leica, Mannheim, Germany) and graphic software (CorelDRAW X3, Corel).
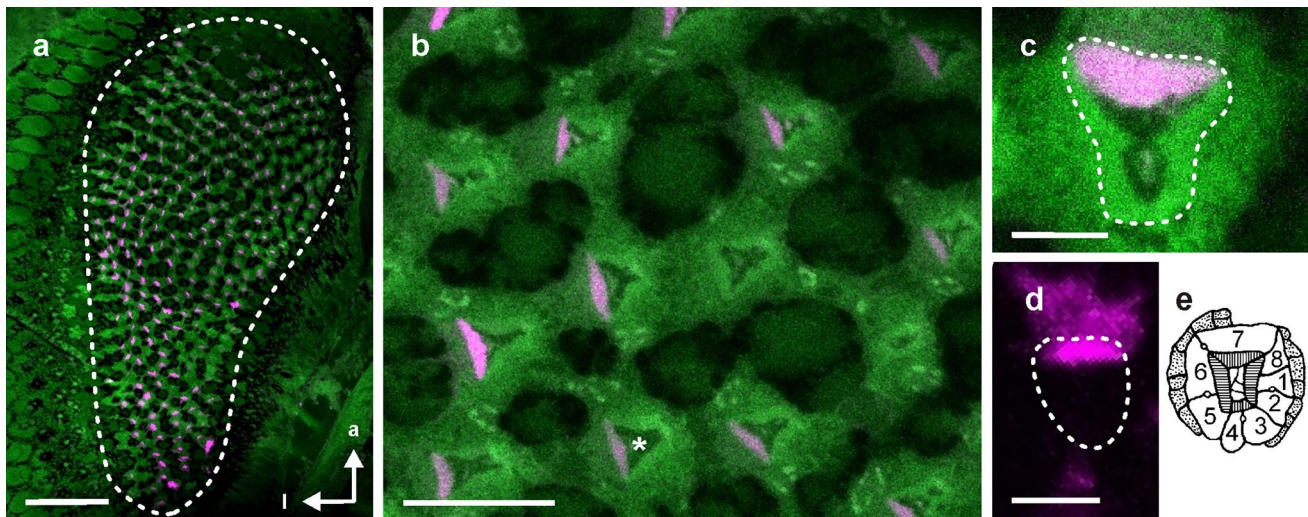
Fig. 1 Retrograde mass staining of DRA photoreceptors. Long visual fibers of the DRA were labeled by injecting dextran-conjugated Texas Red into the dorsal rim of the medulla. Stained photoreceptors are shown in *magenta* against a *green* fluorescent background. Only R7 photoreceptor cells were labeled, indicating that they are the only DRA cells projecting to the dorsal rim of the medulla. **a** Cross section showing the pattern of stained cells in the DRA of the eye. **b** *Detail* from **a**. An *asterisk* marks the position of the crystalline cone in the center of an ommatidium. **c** Cross section of a stained ommatidium. **d** Staining of a single DRA ommatidium. Detection sensitivity of the confocal microscope was adjusted to visualize the weakly stained cell bodies. *Green* background fluorescence was removed for clarity. **e** Schematic drawing of a DRA ommatidium at the height of the sections in **a–d** (from Homberg and Paech 2002). *White dashed lines* indicate the margin of the DRA in **a** and of the rhabdoms in **c** and **d**. *Scale bars* **a**: 100 µm; **b, d** 10 µm; **c** 5 µm. Orientations are indicated by *arrows* (*l* lateral, *a* anterior)

To identify cellular structures and neuropil boundaries or weakly labeled processes, several preparations were scanned multiple times with varying detection sensitivity of the confocal laser scanning microscope. Tissue slices were observed once with low and once with high scanning sensitivity. Thereby, strong and weak fluorescent structures could be distinguished in detail. Information from scans with high and low sensitivity was combined for figure illustration.

Results

Identification of long and short visual fibers of the DRA

Neuronal tracer, injected into the dorsal rim of the medulla, was taken up by photoreceptor axons and was distributed throughout the whole cells. Therefore, all photoreceptors stained at the level of the retina are considered to be long visual fibers terminating in the dorsal rim of the medulla. In contrast, all unlabelled photoreceptor cells are considered short visual fibers. Retinal cross sections demonstrate that it was possible to trace stained photoreceptor profiles across the whole DRA (Fig. 1a). Boundaries of ommatidia were identified by their higher fluorescence compared with the surrounding tissue (Fig. 1b). In contrast, individual unlabelled retinula cells could not be distinguished clearly from each other. The extension of the crystalline cone

appeared as a non-fluorescent area in the center of the rhabdoms (Fig. 1b, c).

In stained photoreceptors, microvillar regions showed considerably stronger fluorescence than the rest of the cell body, which was only visible by raising the detection sensitivity of the confocal scanning process (Fig. 1c, d). In contrast to the highly structured rhabdom, photoreceptor cell margins had highly irregular shapes. Usually one cell per ommatidium was stained, with only few exceptions in which no cell had taken up the tracer (Fig. 1b). Stained cells could be identified as receptor cell R7, using rhabdom shape and microvilli orientation as criteria (Fig. 1c, e; compare Homberg and Paech 2002; Schmeling et al. 2014). The data show that R7 photoreceptors in the DRA are long visual fibers while R1–R6 and R8 are short visual fibers terminating in the lamina.

Optic chiasma and retinotopy within the dorsal rim areas of the lamina and medulla

Anterograde mass staining revealed an optic chiasma of long visual fibers in the horizontal plane between the dorsal rim area of the lamina (DRLA) and medulla (DRME). Axonal projections from the DRA of the eye extended to corresponding positions of the DRLA (Fig. 2a, inset), but long visual fibers terminated in positions of the DRME corresponding to the inversion of the anterior-posterior axis (Fig. 2a, b). Thus, a long visual fiber originating from the
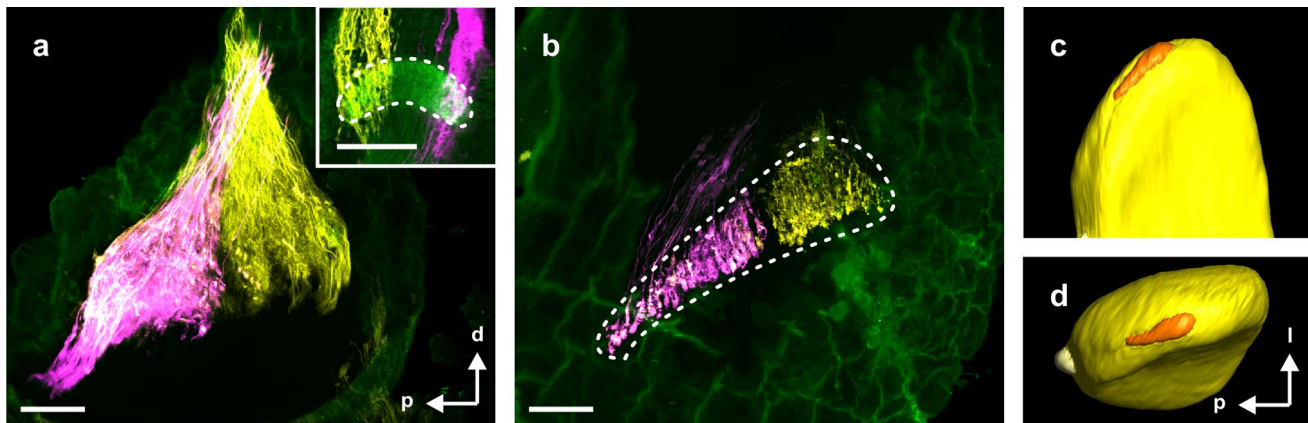
Fig. 2 Anterograde mass staining of long visual fibers projecting from the DRA of the eye to the dorsal rim of the medulla. Two different tracers were injected into the anterior (dextran–Texas *Red*, *magenta*) and posterior (Neurobiotin, *yellow*) part of the DRA. **a** Sagittal section with a slight horizontal angle through the dorsal rim of the medulla. *Inset* shows projections through the DRLA. **b** Sagittal section with a slight horizontal angle from the same optic lobe showing a more ventral region of the dorsal rim of the medulla. **c**, **d** 3D reconstruction of the medulla (*yellow*), including the DRME (*orange*) and the accessory medulla (*light yellow*). Neuropil margins in **a** and **b** are indicated by *dashed lines*. *Scale bars* 50 μm. Orientations (identical **a**, **b** and **c**) are indicated by *arrows* (*d* dorsal, *p* posterior, *l* lateral)

anterior edge of the DRA extended to the anterior DRLA but the continuing neurite changed direction and terminated near the posterior edge of the DRME. The shape of the DRME resembles that of the DRA of the eye with a wide anterior and a more slender posterior part. A 3D reconstruction of the neuropils demonstrates how the DRME is embedded in the medulla (Fig. 2c, d; data from Kurylas et al. 2008). Retinula cell projections end relatively irregularly within the DRME but are largely confined to the upper two-thirds of the DRME (Figs. 2b, 3e, 5c, f).

Single cell stainings following electrophysiological recordings were used to reveal axonal projection patterns along the lateral–medial axis. Figure 3 shows a full histological dataset of a stained R7 retinula cell. It includes information on the cell's position within the DRA, receptor identity, an overview of axonal projections, and details of arborizations within the DRLA (Fig. 3d) and DRME (Fig. 3e).

Retinotopic projections of visual fibers from the DRA to the DRLA and DRME were also obvious in frontal plane, lacking an optic chiasma (Figs. 4, 5). Receptor position within the DRA of the retina strongly correlates with its axonal projection sites in the DRLA and DRME. Receptors in lateral positions of the DRA send their projections to lateral sides of the DRLA and DRME and the more a receptor's position is shifted medially, the more medial are its terminations.

Structure and shape of axonal projections

In general, fine axonal arborizations were spatially confined to a narrow area close to the main axon. Short visual fibers penetrated deeply into the DRLA and gave rise to bulbous, club-like terminals, in some cases with short spiny extensions in close proximity to the main fiber. No indications of synaptic contacts were found throughout the distal half of the DRLA (Fig. 4).

In contrast, long visual fibers had short and usually fine lateral extensions throughout the depth of the DRLA, again in close proximity to the main fiber (Figs. 5b, e, 6a). In the DRME, projection depth varied but the most ventral part of the DRME was usually not invaded (Figs. 3e, 5c, f, 6b). This is consistent with the findings of anterograde mass stainings (Fig. 2). Terminations appeared again prominently varicose. Cases were found in which a bulb of small arborizations originated from the main axon (Figs. 5f; 6b). In other cases, only few short thin fibers seemed to extend from the main axon (Fig. 5c). The uppermost, distal quarter of the DRME was conspicuously free of side branches or termination sites (Fig. 3e, 5c, f, 6b). Between the retina and lamina and within the DRLA, axons of long visual fibers had larger diameters (about 3 μm) than short visual fibers (about 1 μm). After leaving the DRLA, however, axons of long visual fibers abruptly decreased in thickness to about 1 μm (Fig. 6a). The site of change in fiber diameter correlated with a bend in axonal trajectory.

Visual fiber projections in the main eye

Retrograde mass staining from the main medulla, as from the DRME, labeled a single photoreceptor per ommatidium in the main retina (Fig. 7). Cross sections at a deeper level through the axonal bundles leaving the retina, likewise, showed only one stained retinula cell axon per ommatidium
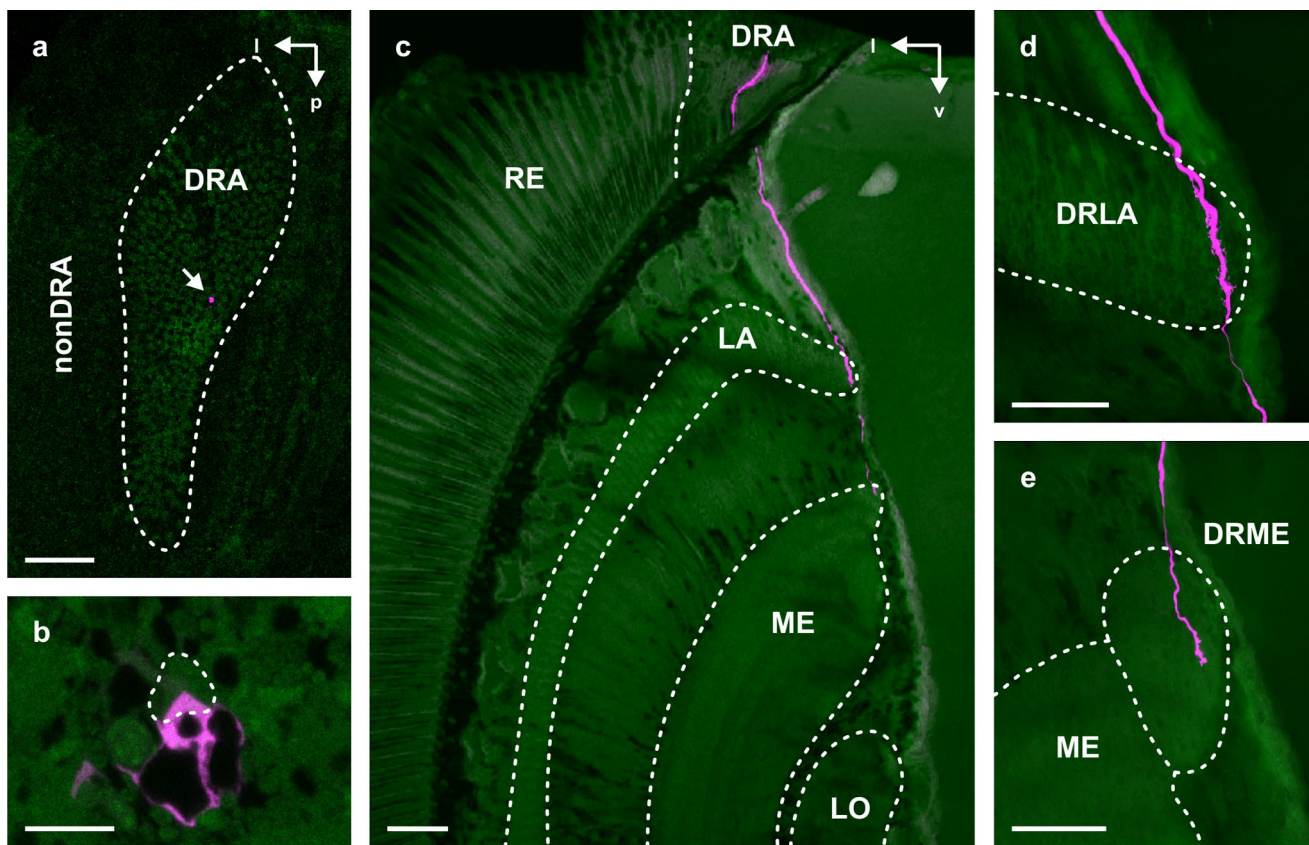
Fig. 3 Staining of a single DRA photoreceptor. Neurobiotin was injected iontophoretically into the receptor cell after electrophysiological recording. The stained R7 photoreceptor (*magenta*) is a long visual fiber with projections through the DRLA and terminal projections in the DRME. **a** Cross section of the DRA. The stained cell is indicated by a *white arrow*. **b** Magnification from (**a**). The size of the cell's rhabdomere, its triangular shape and orientation within the DRA identifies it as an R7 photoreceptor. **c** Frontal section through the optic lobe, showing an overview of the axonal projection of the photoreceptor. *LA* lamina, *LO* lobula, *ME* medulla, *RE* retina. **d, e** Frontal sections through the dorsal rim of the lamina (*DRLA*, **d**) and medulla (*DRME*, **e**). *Scale bars* **a, c** 100 µm; **d, e** 50 µm; **b**: 10 µm. *Dashed lines* show margins of DRA and neuropils. Orientations, identical in **a, b**, and in **c–e**, are indicated by *arrows* (*l* lateral, *p* posterior, *v* ventral)

(data not shown). Two types of ommatidia could be distinguished with the stained photoreceptor pointing either anterior-dorsally or anterior-ventrally within an ommatidium (Fig. 7b, c). Both types were randomly distributed throughout the main eye. A highly similar arrangement of photoreceptors expressing UV and blue opsins in locust ommatidia was recently established by Schmeling et al. (2014). Based on that study, we conclude that the stained cell is R7. Anterograde mass staining further revealed that all long visual fibers terminate in distal layer 3 of the medulla (Fig. 7d). This layer was identified by comparison with observations of Wendt and Homberg (1992) and Gebhardt and Homberg (2004). A horizontally projecting fiber bundle which lies medially from layer 4 (el Jundi et al. 2011) also served as an anatomical landmark for layer identification (asterisk in Fig. 7d). While running through the outer layers of the medulla, receptor axons showed no apparent arborizations until they reached a narrow band of terminations characterized by relatively short and spatially highly aligned bulbous endings (Fig. 7e).

Dye application following intracellular recording from blue/green sensitive photoreceptors consistently ($n = 4$) resulted in co-labeling of 5 stained receptor cells terminating in the lamina but at different depths (Fig. 8). In accordance with Schmeling et al. (2014), those cells were identified as R2, R3, R5, R6, and R8 photoreceptors. These receptors contribute microvilli through the whole length of the rhabdom. In contrast, receptors R1, R4, and R7 remained unstained. R7 is a distal photoreceptor, while R1 and R4 are proximal photoreceptors (Wilson et al. 1978; Schmeling et al. 2014).

Receptive fields

Recording data were collected from gregarious and solitarious locusts. From the center of the receptive fields, the relative sensitivity decreased with increasing distance in an
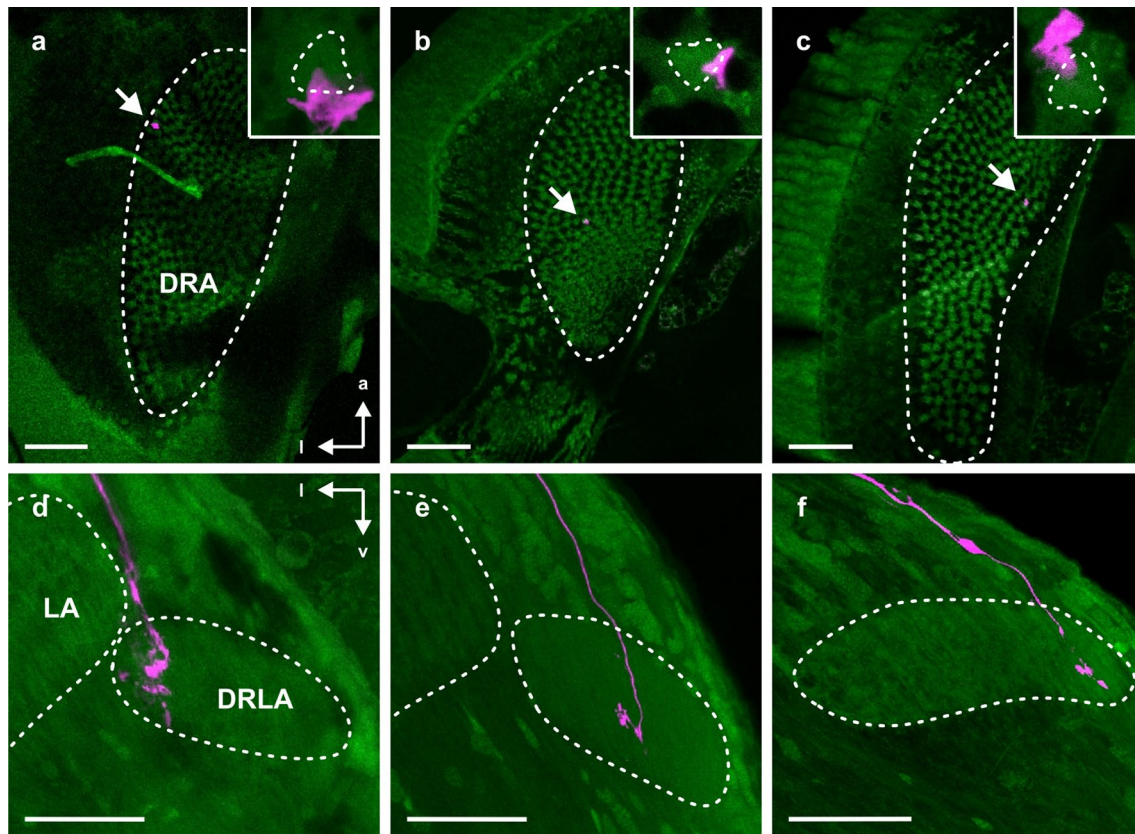
Fig. 4 Axonal projections of short visual fibers from the DRA to the DRLA. Single cell stainings demonstrate retinotopy across the medio-lateral axis. **a–c** Cross sections of the DRA with single cells stained (*white arrows*). *Insets* show magnifications of the corresponding images, revealing the identity of photoreceptors as R1 (**a**) and R1 or R2 (**b, c**). **d–f** Frontal sections through the DRLA showing axonal projections (*magenta*) of the receptors in **a–c**. For neuropil background staining, a synapsin antibody with Cy5 as fluorophore was used. *White dashed lines* show outlines of the DRA (**a–c**) and the LA and DRLA (**d–f**). *Scale bars* 50 µm. Orientation of figures is identical in **a–c** and **d–f** (*l* lateral, *a* anterior, *v* ventral)

exponential manner (Fig. 9), as has been observed in other insects (Labhart 1980; Labhart et al. 1984; Stalleicken et al. 2006). The two main parameters of a receptive field are its acceptance angle and its total extent. The acceptance angle (half-width of angular sensitivity) was further used for statistical tests. The visual fields within the acceptance angle appear symmetrically shaped in the DRA and main eye, and no significant difference in acceptance angle width was found along the lateral–medial and anterior–posterior axis as well as between gregarious and solitarious locusts (gregarious: $n = 10$ DRA, $n = 22$ main eye; solitarious: $n = 7$ DRA, $n = 10$ main eye). Data were, therefore, pooled. The average acceptance angle of DRA receptors was 33° (±18.6°), and of receptors of the main eye, 2.04° (±1.3°). The widest visual field extent of a single receptor in the DRA was 149° and 43° in the main retina. Especially in the main retina, a relatively small center of high sensitivity could be distinguished from a wide surrounding region of extremely low sensitivity (falling below 10 % when exceeding 8°, Fig. 9b), which matches observations in the bee (Labhart 1980).

While the receptive fields beyond the acceptance angle were circularly shaped in the main retina, there was often a remarkable asymmetry in the DRA, especially along the lateral–medial axis. Often receptor sensitivity decreased more strongly in medial than in lateral direction. This effect can be seen even in the averaged curves in Fig. 9a. All receptive field centers of DRA photoreceptors point contralaterally. An estimate of the DRA's total visual field was obtained by overlaying measurements of all recorded receptors (Fig. 10). The visual field of the DRA (at 50 % sensitivity) is 80° along the lateral–medial axis and 100° across the anterior–posterior axis. Its total width is 160° dorso-ventrally and posterior–anteriorly and thereby covers almost the whole dorsal hemisphere.

Discussion

Photoreceptor projections and their receptive fields differ in several aspects between the DRA and main retina of
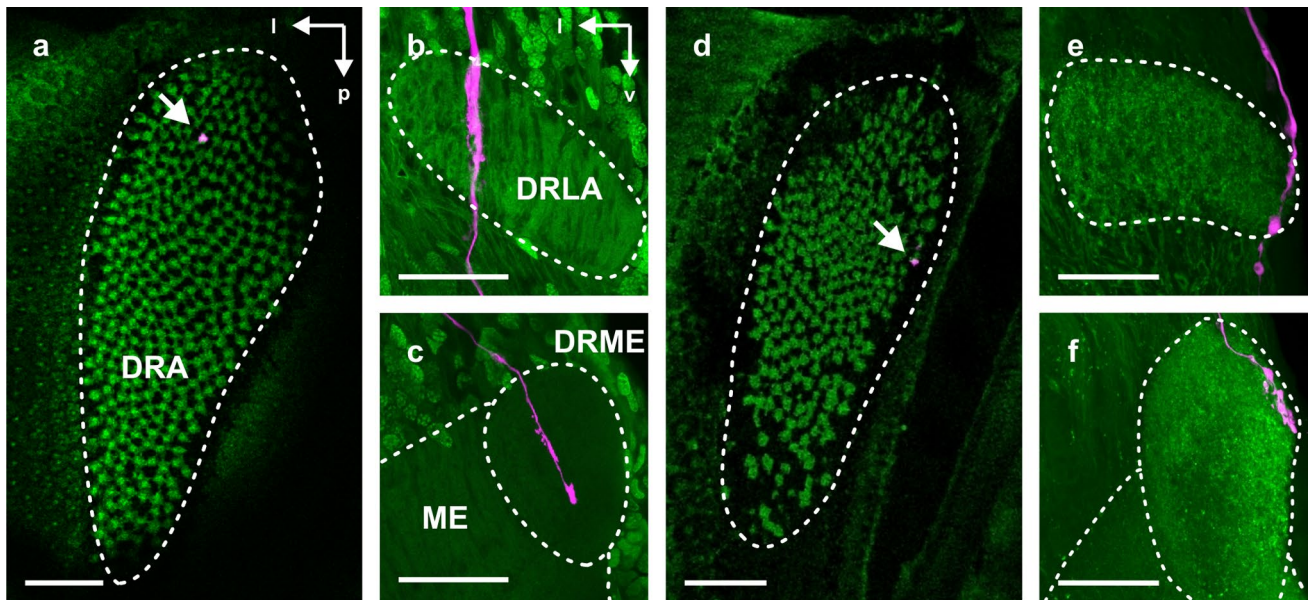
Fig. 5 Axonal projections of long visual fibers to the DRLA and DRME. As for short visual fibers, stainings demonstrate retinotopic projections. **a, d** Cross sections of the DRA with single cells stained (*white arrow*). **b, c** and **e, f** Frontal sections through the DRLA and DRME showing axonal projections (*magenta*) of the receptors in **a** and **d**. *Scale bars* **a, d** 100 μm; **b, c, e, f** 50 μm. Orientation is identical in **a, d** and **b, c, e, f** (*l* lateral, *p* posterior, *v* ventral)
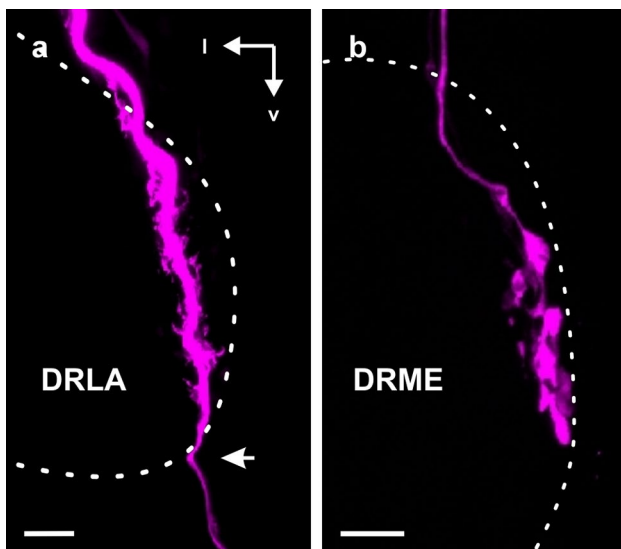

Fig. 6 Details of R7 photoreceptor projections from the DRA. **a** Fine short arborizations cover the whole length of the axon in the DRLA. The axon diameter decreases greatly after a strong bend (indicated by *arrow*), when leaving the neuropil. **b** Axonal projections (from a different preparation) terminate in the form of small knots within the DRME. Orientations, identical in **a** and **b**, are indicated by *arrows* (*l* lateral, *v* ventral). *Scale bars* 10 μm

the desert locust, while other features show similarities. In both eye regions, a single retinula cell per ommatidium, identified as R7, projects a long visual fiber to the medulla, whereas R1–R6 and R8 are short visual fibers terminating

in the lamina. As in the main visual system, retinotopy of photoreceptor projections is maintained in the DRLA and DRME. The receptive fields of DRA receptors are about 180 times larger in area than those of receptors from the main eye. In contrast to the ipsilateral visual field of the main eye, the DRA as a whole covers an ellipsoid visual field of roughly 80° × 100° in the contralateral visual field near the zenith.

Central projections of DRA photoreceptors

As in the cricket (Blum and Labhart 2000), each ommatidium of the DRA of the locust *S. gregaria* contains only one long visual fiber, R7 (Fig. 1), while the remaining cells have short fibers terminating in the lamina. Projections of photoreceptors to the DRLA and DRME are retinotopically organized and, in case of R7 photoreceptors, follow the fiber crossings of the first optic chiasm, despite the fact that both neuropils appear relatively unstructured and show no layer arrangement as seen in the main medulla (Fig. 7d). Retinotopic organization of the DRME would allow for spatially distinct input to postsynaptic transmedulla neurons projecting to the lower division of the anterior optic tubercle (Homberg et al. 2003), but the ramification patterns of those interneurons in the DRME have not yet been determined.

At the level of the DRLA, long and short visual fibers strongly differ in their morphology. The axons of long visual fibers have considerably larger diameters than
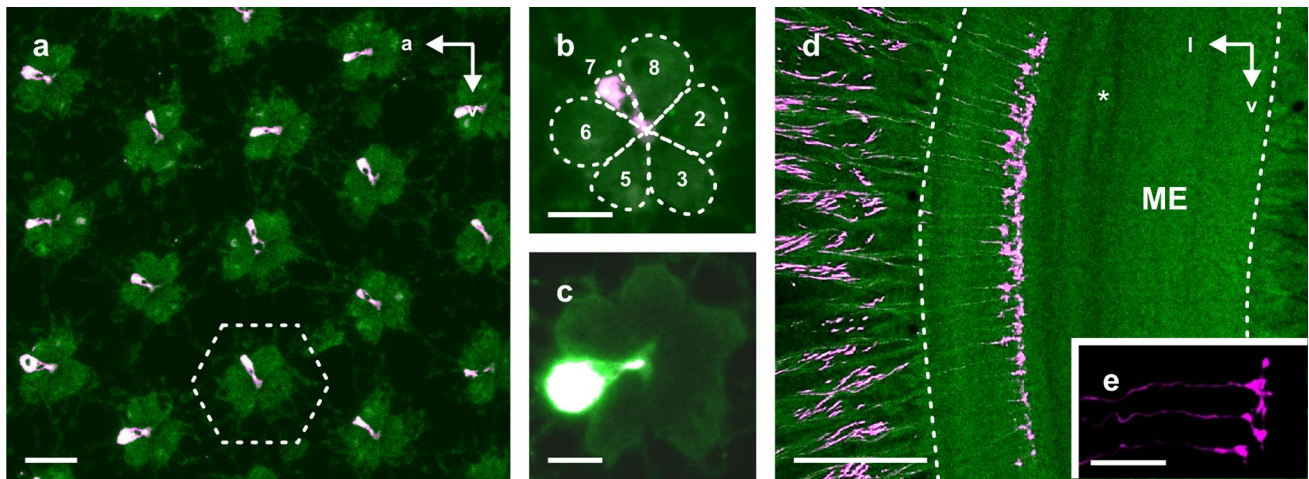
Fig. 7 Retrograde and anterograde mass staining of photoreceptors of the main retina. Long visual fibers were labelled by injecting dextran–Texas Red into the medulla or the retina. Stained photoreceptors are shown in *magenta*; background staining originates from synapsin labelling (*green*). Exclusively R7 receptor cells are stained, indicating that they are the only cells with long visual fibers projecting to the medulla, terminating in layer 3. **a** Cross section of the main retina showing stained photoreceptors in two different orientations within the ommatidia, either pointing anterior-dorsally or anterior-ventrally. *Dashed line* outlines a corresponding facet. **b** Details of a single ommatidium with the stained cell pointing anterior-dorsally.

Dashed lines outline the retinula cells of the ommatidium. **c** Details of the second type of ommatidium with the stained cell pointing anterior-ventrally (cross section 8 μm). **d** Frontal section through the *ME* showing an overview of axonal projections. **e** Details of axonal terminals. *Dashed lines* indicate the *ME* boundaries. An *asterisk* marks a horizontally projecting fiber bundle which lies medially from layer 4 and was used as an anatomical landmark for layer definition. *Scale bars* **a** 10 μm; **b, c**: 5 μm; **d** 100 μm; **e** 25 μm. Orientations are indicated by *arrows* and are identical in **a–c** (*a* anterior, *l* lateral, *v* ventral)
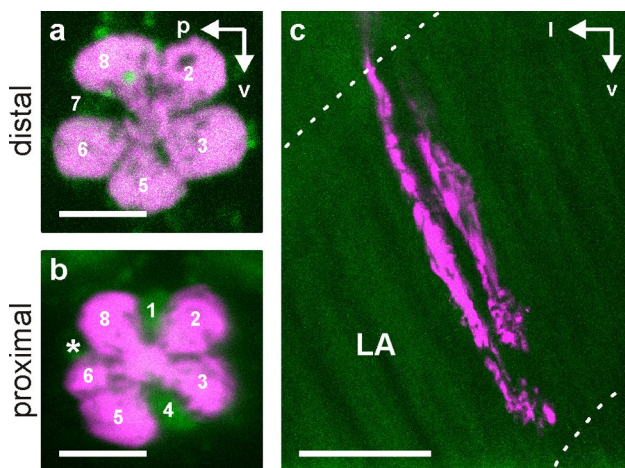

Fig. 8 Axonal projections of short visual fibers from the main retina to the lamina. Five receptor cells (R2, R3, R5, R6, and R8) were co-labelled following Neurobiotin injection after single-cell intracellular recording. The long photoreceptor R7 and the two proximal receptors R1 and R4 remained unlabelled. At least two axon bundles with different lengths can be recognized. **a–b** Cross sections of the retina at a distal (**a**) and proximal (**b**) level of the rhabdom. **c** Frontal section through the lamina (*LA*). The *asterisk* in **b** indicates the position of R7. *Scale bars* **a, b** 5 μm; **c** 25 μm

short visual fibers and, thus, should show a smaller decrement of light-induced depolarizations along their axons. As a consequence, they should reach critical levels of

depolarizations at synaptic release sites faster than the short fibers. This may be of functional relevance considering the mechanisms proposed to underlie polarization opponency (Labhart and Petzold 1993; Wehner and Labhart 2006). Many polarization-sensitive interneurons in the brain of locusts, crickets and other insects receive excitatory input at a particular *E*-vector orientation, termed Φ_{max}, and inhibitory input at orthogonal *E*-vector orientation, Φ_{min} (Labhart and Meyer 2002; Homberg et al. 2011). This property, termed polarization opponency, may arise from antagonistic processing and convergence of inputs from the two sets of photoreceptors with orthogonal microvilli orientations in each DRA ommatidium (Wehner 1982; Labhart 1988). Insect photoreceptors, including those of the locust DRA, use histamine as a neurotransmitter (Hardie 1987, 1989; Nässel 1999; Gebhardt and Homberg 2004). Light-induced histamine release leads to opening of chloride channels resulting in neuronal inhibition. Polarization opponency, however, requires one of the two input channels to be excitatory. This could be achieved by an intercalated interneuron switching the photoreceptor's effect on a DRLA polarization opponent interneuron to excitation. Because an intercalated interneuron would lead to a delay in information processing, compensation by a larger axon diameter and, thus, faster depolarization at synapses in the indirect input channel to the polarization opponent interneuron may be a way to assure that the opponent inputs arrive at the same
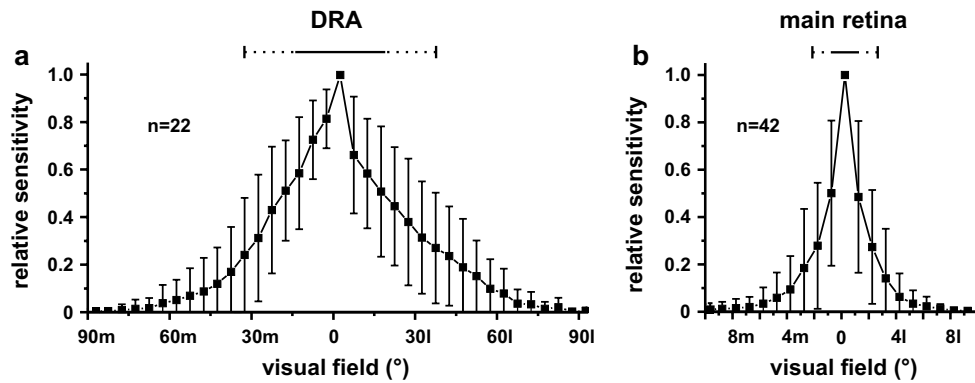
Fig. 9 Receptive fields (means, SD) of photoreceptors from the DRA (**a**) and main retina (**b**). Relative sensitivities are plotted as a function of binned positions (5° bins in **a**; 1° bins in **b**) of the stimulus. Visual fields in the DRA are considerably larger than in the main retina, while the shapes are similar. With increasing distance medially (*m*) and laterally (*l*) from the visual center, relative sensitivity decreases in an exponential manner. The averaged acceptance angles (*solid lines*) and their standard deviations (*dotted lines*) are indicated by the bars above the graphs
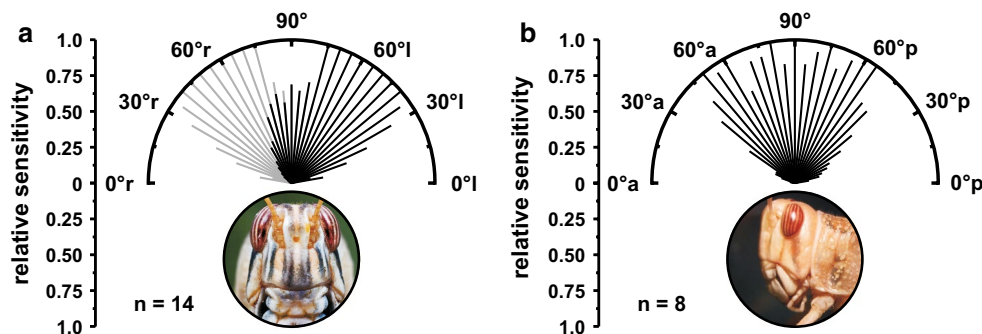

Fig. 10 Overlays of all single visual fields measured in the DRA. Relative sensitivities are plotted as a function of binned positions (5° bins) of the stimulus. **a** Visual field extensions along the medial–lateral axis. The *black bars* indicate relative sensitivity distributions of pooled right eye photoreceptors. Measurements from the left eye were mirrored and added. Pooled data were mirrored to indicate the visual field of the left DRA (*gray bars*). **b** Visual field extensions along the anterior–posterior axis. Data from gregarious and solitarious locusts were pooled with *n* indicating the number of recorded cells. (*r* right, *l* left, *a* anterior, *p* posterior)

time. R7 would, therefore, be an attractive candidate photoreceptor in the indirect longer pathway mediating excitatory input to polarization opponent interneurons at the level of the DRLA.

Another main difference between short and long visual fibers concerns the distribution of arborizations in the DRLA. Axonal side branches were found over the whole length of the long visual fibers but were basically absent in short visual fibers in the distal half of the DRLA. What are the postsynaptic partners of long visual fibers in the more distal region of the DRLA? An additional neuron type could be the answer to that question. The neuronal elements of the lamina subserving the main eye of *S. gregaria* have been studied by Nowel and Shelton (1981). They reported similar differences between long and short visual fibers, as shown here, concerning details of finer arborizations.

Differences in length between short visual fibers and in the position of their finer arborizations, as reported by Nowel and Shelton (1981) for the main eye, have not been found by us in the DRLA.

When leaving the DRLA, long visual fibers show an abrupt reduction in fiber diameter, which might again be relevant for coincident integration of polarization opponent input in the DRME. The single cell stainings confirmed the findings of mass stainings (Fig. 2b) that long visual fibers usually do not extend fully through the DRME. Final terminations are located at about the last two-thirds of the fiber, which differs strongly from the locally more narrow terminations of long visual fibers in the main medulla. This might be due to the fact that no obvious layering occurs in the DRME, while the main medulla appears heavily structured (Gebhardt and Homberg 2004).

Photoreceptors of the main retina

In the main retina as in the DRA, only R7 was identified as a long visual fiber (Fig. 7). This contrasts with earlier findings by Horridge and Meinertzhagen (1970) and Nowel and Shelton (1981) who reported two long visual fibers in *S. gregaria*. In the first publication, photoreceptor projections were traced through the first optic chiasma on transverse sections of axonal tissue but the authors did not provide original data for the locust. Nowel and Shelton (1981) distinguished two morphological types of long visual fibers based on Golgi impregnations but whether these two types are present in the same ommatidium was not addressed. Using the same technique and premise as Nowel and Shelton (1981), Ribi (1975a) reported three long visual fibers in the desert ant, but that was later corrected to two long fibers by Meyer (1984), who used a retrograde staining technique similar to ours. The question arises whether retinula cell axon morphology is sufficient to conclude on the contributing ommatidium. In view of our current data, together with evidence from Schmeling et al. (2014) indicating that two types of ommatidia exist with an R7 photoreceptor expressing either a blue or a UV opsin gene, it may be more likely that the two types of long visual fibers reported by Nowel and Shelton (1981) are in fact the two spectral types of R7 photoreceptors occurring in different ommatidia throughout the main eye. Two different types of R7 (and R8) distributed over the retina are also present in the fruit fly (Wernet and Desplan 2004).

Two long visual fibers have been reported most often in pterygote insects (Strausfeld 1971; Pollack and Hofbauer 1991; Ribi 1975b; Wolburg-Buchholz 1979; Armett-Kibel and Meinertzhagen 1985; Fischbach and Dittrich 1989; Zufall et al. 1989), but cases of three long visual fibers per ommatidium are also known (Shimohigashi and Tominaga 1991; Greiner et al. 2004; Takemura et al. 2005; Paulk et al. 2009), as well as the total absence of long fibers (Buschbeck et al. 2003). Interestingly in the insect species studied so far, R7 is usually among the long visual fibers (together with R8), while R1–R6 are short visual fibers, but again, several exceptions occur, including eye region-specific and sex-specific differences (e.g., Hardie et al. 1981).

Long visual fibers usually terminate in distal layers of the medulla. In the few cases in which termination sites were identified, they occurred in medulla layer 2 (honeybee: Ribi and Scheel 1981; bumblebee: Paulk et al. 2009), layer 2 and 3 (a nocturnal bee: Greiner et al. 2004), layer 4 (butterfly: Hamanaka et al. 2013) or 3 and 6 (fruit fly: Takemura et al. 2008). Terminations of all long visual fibers in the locust medulla occur in a single layer, as illustrated in Fig. 7d. This has also been observed in histamine immunostaining (Gebhardt and Homberg 2004). Gebhardt and Homberg (2004) reported that histamine-immunostained terminals of long visual fibers were confined to layer 4 of the medulla, but careful comparison with the layering of the locust medulla established by Wendt and Homberg (1992) reveals a slightly more distal position in layer 3.

In *S. gregaria*, R2-3 and R5-6 are short visual fibers as in other insect species (Fig. 8) but, in contrast to many other insects, R8 also terminates in the lamina. The axons of these five short visual receptors form two bundles which terminate at different depths of the lamina. This fits to the findings by Nowel and Shelton (1981), based on Golgi impregnations, that short visual fibers differ in their depth of penetration of the lamina. This may imply synaptic connection patterns to different lamina monopolar and horizontal cells (Nowel and Shelton 1981) or even to different transmedulla neurons which in some cases arborize in certain depths of the lamina (Homberg and Würden 1997). Dye injection following intracellular recording of one of these receptors consistently stained the complete set of five photoreceptor cells. A likely explanation is electrical coupling of photoreceptors, which has already been suggested for locust photoreceptors through physiological recordings (Shaw 1967, 1969; Lillywhite 1978). All co-labeled receptors directly contact each other at the distal region of the ommatidium (Fig. 8a), but gap junctions may of course also occur in the region of the rhabdom. All five dye-coupled receptors (R2, R3, R5, R6, R8) contain blue as well as green opsin (Schmeling et al. 2014) supporting a common functional role. The receptors R1 and R4 could not be stained in any of the recordings. Both receptors are green sensitive (Schmeling et al. 2014) and, judged from the mass backfill experiments (Fig. 7), are short visual fibers.

The color vision system of many insects consists of two long visual fibers, UV or blue sensitive, and green sensitive short visual fibers (Zufall et al. 1989; Briscoe et al. 2003; White et al. 2003; Spaethe and Briscoe 2005; Wakakuwa et al. 2005). A similar trichromatic color vision system may be present in the desert locust consisting of UV and blue sensitive long visual fibers (in different ommatidia) and green sensitive short visual fibers (in each ommatidium; Schmeling et al. 2014). The observation that the UV or blue photoreceptor R7 in *S. gregaria* has a rhabdomere confined to distal parts of the ommatidium, whereas the two green receptors only contribute to the rhabdom proximally (Schmeling et al. 2014), may support their adaptation to vision at daylight intensities, and is similar to the situation in the migratory locust (Wilson et al. 1978).

Receptive fields

With a mean acceptance angle of 33° in the DRA and 2.04° in the main retina, the photoreceptors in *S. gregaria* have similar angular sensitivities as those of the field cricket *Gryllus campestris* (DRA: 10°–35°, main retina: 6°; Labhart

et al. 1984) and the migratory locust in dark adapted state (main retina: 2.8°; Williams 1983). Certain other insect species show considerably smaller acceptance angles in their DRA, down to about 4° (bee: Labhart 1980; ant: Labhart 1986; butterfly: Stalleicken et al. 2006). The large angular sensitivity in the locust DRA correlates with anatomical specializations of the optic apparatus, like absence of screening pigment and the presence of light scattering structures (Homberg and Paech 2002). This way more photons can be collected from DRA receptors, compared with receptors from the main eye, resulting in enhanced overall light sensitivity. The receptive fields of locust DRA receptors are about 180 times larger than those of receptors in the main eye, suggesting a similar increase in sensitivity (compare Schmeling et al. 2014, Fig. 8). Considering receptive field size, a factor of 600 was found in a cricket by Zufall (1984). When stimulating with small light spots, cricket DRA receptors were less sensitive than receptors in the main retina, but considering their wider receptive field, Zufall et al. (1989) concluded that cricket DRA receptors are actually 60 times more sensitive to an extended source of light.

Summing up the receptive fields of all receptors in both DRAs, three facts become apparent: (1) the combined visual fields cover most parts of the sky, (2) the visual field is limited to areas above the horizon, and (3) the relative sensitivity of each DRA at the zenith is only about 50 % but here, both DRAs overlap in their visual fields. The main effect of the large size of the visual field is that the celestial polarization pattern is detected as completely as possible. Especially during inhomogeneous sky conditions, this might be an advantage. Even if the celestial *E*-vector pattern is partly occluded by clouds, as many free spots as possible in the sky would lie within the DRAs' visual field and can contribute to solar azimuth signaling, thereby enhancing accuracy (Labhart 1999). The large visual fields are, moreover, a prerequisite for matched filter properties of polarization-sensitive neurons in the central brain and may allow the solar and anti-solar hemispheres of the sky to be distinguished, particularly at higher solar elevations (Bech et al. 2014). Interestingly, a complete view of the sky is not always present in insect species sensitive to the sky polarization pattern. The DRAs of the monarch butterfly and desert ant have rather narrow visual fields (Stalleicken et al. 2006; Labhart 1986). However, the intuitive conclusion that monarch butterflies possess an inferior polarization detecting system compared to locusts has still to be proven. It has to be kept in mind that insects use several celestial cues for orientation, complementing each other, but with different weight. Perhaps polarized light plays a dominant role in locusts, as in ants (Wehner and Müller 2006), while in monarch butterflies the position of the sun may be the most important cue (Mouritsen et al. 2013; Oberhauser et al. 2013).

S. gregaria do not only detect polarized light from above but also show a behavioral response, when polarized light is presented from below (Shashar et al. 2005; el Jundi and Homberg 2010). With receptors basically looking upwards, the DRA is unlikely to provide the explanation for this polarization sensitivity. In this case, polarized light is more likely to be detected by photoreceptors of the main eye. The visual field of the main eye covers regions below the horizon and might show sufficient polarization sensitivity even with low PS values (Schmeling et al. 2014) as discussed by Wernet et al. (2012).

Whether the relatively low sensitivity of the DRA in the zenith (Fig. 10a) serves a particular function remains unclear. However, despite the relatively weak sensitivities of each single DRA in this region, their combined overlapping visual fields still may provide sufficient signal amplitude to accurately detect zenithal *E*-vector orientations, leaving no blind spot. In fact relative sensitivity in the zenith is about 50 % for each DRA, which would sum up to 100 %, when signals from both eyes are combined. The asymmetrically shaped visual field of the locust DRA might result from the fact that the head capsule limits receptor sight in the contralateral direction that results in a rapid decrease of sensitivity contralaterally to the receptors' visual field center. No obstacles occur ipsilaterally, and visual sensitivity decreases gradually. This effect is still recognizable in the averaged measurements (Fig. 9) and adds up when observing the DRA's whole visual field (Fig. 10a).

References

Armett-Kibel C, Meinertzhagen IA (1985) The long visual fibers of the dragonfly optic lobe: their cells of origin and lamina connections. J Comp Neurol 242:459–474

Bech M, Homberg U, Pfeiffer K (2014) Receptive fields of locust brain neurons are matched to polarization patterns of the sky. Curr Biol 24:2124–2129

Blum M, Labhart T (2000) Photoreceptor visual fields, ommatidial array, and receptor axon projections in the polarisation-sensitive dorsal rim area of the cricket compound eye. J Comp Physiol A 186:119–128

Briscoe AD, Bernard GD, Szeto AS, Nagy LM, White RH (2003) Not all butterfly eyes are created equal: rhodopsin absorption spectra, molecular identification, and localization of ultraviolet-, blue-, and green-sensitive rhodopsin-encoding mRNAs in the retina of *Vanessa cardui*. J Comp Neurol 458:334–349

Brunner D, Labhart T (1987) Behavioural evidence for polarization vision in crickets. Physiol Entomol 12:1–10

Burkhardt D, Streck P (1965) Das Sehfeld einzelner Sehzellen: Eine Richtigstellung. Z Vgl Physiol 51:151–152

Buschbeck EK, Ehmer B, Hoy RR (2003) The unusual visual system of the Strepsiptera: external eye and neuropils. J Comp Physiol A 189:617–630

Dacke M, Nordström P, Scholtz C (2003) Twilight orientation to polarized light in the crepuscular dung beetle *Scarabaeus zambesianus*. J Exp Biol 206:1535–1543

el Jundi B, Homberg U (2010) Evidence for the possible existence of a second polarization-vision pathway in the locust brain. J Insect Physiol 56:971–979

el Jundi B, Homberg U (2012) Receptive field properties and intensity-response functions of polarization-sensitive neurons of the optic tubercle in gregarious and solitarious locusts. J Neurophysiol 108:1695–1710

el Jundi B, Pfeiffer K, Homberg U (2011) A distinct layer of the medulla integrates sky compass signals in the brain of an insect. PLoS One 6:e27855

Fischbach KF, Dittrich APM (1989) The optic lobe of *Drosophila melanogaster*. I. A Golgi analysis of wild-type structure. Cell Tissue Res 258:441–475

Gebhardt S, Homberg U (2004) Immunocytochemistry of histamine in the brain of the locust *Schistocerca gregaria*. Cell Tissue Res 317:195–205

Greiner B, Ribi WA, Wcislo WT, Warrant EJ (2004) Neural organization in the first optic ganglion of the nocturnal bee *Megalopta genalis*. Cell Tissue Res 318:429–437

Hamanaka Y, Shibasaki H, Kinoshita M, Arikawa K (2013) Neurons innervating the lamina in the butterfly, *Papilio xuthus*. J Comp Physiol A 199:341–351

Hardie RC (1987) Is histamine a neurotransmitter in insect photoreceptors? J Comp Physiol A 161:201–213

Hardie RC (1989) A histamine-activated chloride channel involved in neurotransmission at a photoreceptor synapse. Nature 339:704–706

Hardie RC, Franceschini N, Ribi W, Kirschfeld K (1981) Distribution and properties of sex-specific photoreceptors in the fly *Musca domestica*. J Comp Physiol A 145:139–152

Heinze S, Homberg U (2008) Neuroarchitecture of the central complex of the desert locust: intrinsic and columnar neurons. J Comp Neurol 511:454–478

Homberg U, el Jundi B (2013) Polarization vision in arthropods. In: Werner JS, Chalupa LM (eds) The new visual neurosciences. MIT Press, Cambridge, pp 1207–1217

Homberg U, Paech A (2002) Ultrastructure and orientation of ommatidia in the dorsal rim of the locust compound eye. Arthropod Struct Dev 30:271–280

Homberg U, Würden S (1997) Movement-sensitive, polarization-sensitive, and light-sensitive neurons of the medulla and accessory medulla of the locust, *Schistocerca gregaria*. J Comp Neurol 386:329–346

Homberg U, Hofer S, Pfeiffer K, Gebhardt S (2003) Organization and neural connections of the anterior optic tubercle in the brain of the desert locust, *Schistocerca gregaria*. J Comp Neurol 462:415–430

Homberg U, Heinze S, Pfeiffer K, Kinoshita M, el Jundi B (2011) Central neural coding of sky polarization in insects. Philos Trans R Soc B 366:680–687

Horridge GA, Meinertzhagen IA (1970) The exact neural projection of the visual fields upon first and second ganglia of the insect eye. Z Vgl Physiol 66:369–378

Horváth G, Varjú D (2004) Polarized light in animal vision: Polarization patterns in nature. Springer, Heidelberg

Klagges BR, Heimbeck G, Godenschwege TA, Hofbauer A, Pflugfelder GO, Reifegerste R, Reisch D, Schaupp M, Buchner S, Buchner E (1996) Invertebrate synapsins: a single gene codes for several isoforms in *Drosophila*. J Neurosci 16:3154–3165

Kurylas AE, Rohlfing T, Krofczik S, Jenett A, Homberg U (2008) Standardized atlas of the brain of the desert locust, *Schistocerca gregaria*. Cell Tissue Res 333:125–145

Labhart T (1980) Specialized photoreceptors at the dorsal rim of the honeybee's compound eye: polarizational and angular sensitivity. J Comp Physiol A 141:19–30

Labhart T (1986) The electrophysiology of photoreceptors in different eye regions of the desert ant *Cataglyphis bicolor*. J Comp Physiol A 158:1–7

Labhart T (1988) Polarization-opponent interneurons in the insect visual system. Nature 331:435–437

Labhart T (1999) How polarization-sensitive interneurons of crickets see the polarization pattern of the sky: a field study with an opto-electronic model neuron. J Exp Biol 202:757–770

Labhart T, Meyer E (1999) Detectors for polarized skylight in insects: a survey of ommatidial specializations in the dorsal rim area of the compound eye. Microsc Res Tech 47:368–379

Labhart T, Meyer E (2002) Neural mechanism in insect navigation: polarization compass and odometer. Curr Opin Neurobiol 12:707–714

Labhart T, Petzold J (1993) Processing of polarized light information in the visual system of crickets. In: Wiese K, Gribakin FG, Popov AV, Renninger G (eds) Sensory systems of arthropods. Birkhäuser, Basel, pp 158–169

Labhart T, Hodel B, Valenzuela I (1984) The physiology of the cricket's compound eye with particular references to the anatomically specialized dorsal rim area. J Comp Physiol A 155:289–296

Lillywhite PG (1978) Coupling between locust photoreceptors revealed by study of quantum bumps. J Comp Physiol A 125:13–27

Mappes M, Homberg U (2004) Behavioral analysis of polarization vision in tethered flying locusts. J Comp Physiol A 190:61–68

Meyer EP (1984) Retrograde labeling of photoreceptors in different eye regions of the compound eye of bees and ants. J Neurocytol 13:825–836

Mouritsen H, Derbyshire R, Stalleicken J, Mouritsen OØ, Frost BJ, Norris DR (2013) An experimental displacement and over 50 years of tag-recoveries show that monarch butterflies are not true navigators. Proc Natl Acad Sci 110:7348–7353

Nässel DR (1999) Histamine in the brain of insects: a review. Microsc Res Tech 44:121–136

Nowel MS, Shelton PMJ (1981) A Golgi-electron-microscopical study of the structure and developement of the lamina ganglionaris of the locust optic lobe. Cell Tissue Res 216:377–401

Oberhauser KS, Taylor OR, Reppert SM, Dingle H, Nail KR, Pyle RM, Stenoien C (2013) Are monarch butterflies true navigators? The jury is still out. Proc Natl Acad Sci 110:E3680

Paulk AC, Dacks AM, Gronenberg W (2009) Color processing in the medulla of the bumblebee (Apidae: *Bombus impatiens*). J Comp Neurol 513:441–456

Pollack I, Hofbauer A (1991) Histamine-like immunoreactivity in the visual system and brain of *Drosophila melanogaster*. Cell Tissue Res 226:391–398

Reppert SM, Zhu H, White RH (2004) Polarized light helps monarch butterflies navigate. Curr Biol 14:155–158

Ribi WA (1975a) Golgi studies of the first optic ganglion of the ant, *Cataglyphis bicolor*. Cell Tissue Res 160:207–217

Ribi WA (1975b) The first optic ganglion of the bee. Cell Tissue Res 165:103–111

Ribi WA, Scheel M (1981) The second and third optic ganglia of the worker bee. Cell Tissue Res 221:17–43

Schmeling F, Wakakuwa M, Tegtmeier J, Kinoshita M, Bockhorst T, Arikawa K, Homberg U (2014) Opsin expression, physiological characterization and identification of photoreceptor cells in the dorsal rim area and main retina of the desert locust, *Schistocerca gregaria*. J Exp Biol 217:3557–3568

Shashar N, Sabbah S, Aharoni N (2005) Migratory locusts can detect polarized reflections to avoid flying over the sea. Biol Lett 1:472–475

Shaw SR (1967) Simultaneous recording from two cells in the locust retina. Z Vgl Physiol 55:183–194

Shaw SR (1969) Interreceptor coupling in ommatidia of drone honeybee and locust compound eyes. Vis Res 9:999–1029

Shimohigashi M, Tominaga Y (1991) Identification of UV, green and red receptors, and their projection to lamina in the cabbage butterfly, *Pieris rapae*. Cell Tissue Res 263:49–59

Simpson S, McCaffery A, Hägele BF (1999) A behavioural analysis of phase change in the desert locust. Biol Rev 74:461–480

Spaethe J, Briscoe AD (2005) Molecular characterization and expression of the UV opsin in bumblebees: three ommatidial subtypes in the retina and a new photoreceptor organ in the lamina. J Exp Biol 208:2347–2361

Spurr AR (1969) A low-viscosity epoxy resin embedding medium for electron microscopy. J Ultrastruct Res 26:31–43

Stalleicken J, Labhart T, Mouritsen H (2006) Physiological characterization of the compound eye in monarch butterflies with focus on the dorsal rim area. J Comp Physiol A 192:321–331

Strausfeld NJ (1971) The organization of the insect visual system (light microscopy) - I. Projections and arrangements of neurons in the lamina ganglionaris of Diptera. Z Zellforsch 121:377–441

Takemura S-Y, Kinoshita M, Arikawa K (2005) Photoreceptor projection reveals heterogeneity of lamina cartridges in the visual system of the Japanese yellow swallowtail butterfly, *Papilio xuthus*. J Comp Neurol 483:341–350

Takemura S-Y, Lu Z, Meinertzhagen IA (2008) Synaptic circuits of the *Drosophila* optic lobe: the input terminals to the medulla. J Comp Neurol 509:493–513

von Frisch K (1949) Die Polarisation des Himmelslichts als orientierender Faktor bei den Tänzen der Biene. Experientia 5:142–148

von Philipsborn A, Labhart T (1990) A behavioural study of polarization vision in the fly, *Musca domestica*. J Comp Physiol A 167:737–743

Wakakuwa M, Kurasawa M, Giurfa M, Arikawa K (2005) Spectral heterogeneity of honeybee ommatidia. Naturwissenschaften 92:464–467

Wehner R (1982) Himmelsnavigation bei Insekten: Neurophysiologie und Verhalten. Neujahrsblatt Naturforsch Ges Zürich 184:1–132

Wehner R, Labhart T (2006) Polarization vision. In: Warrant E, Nilsson D-E (eds) Invertebrate Vision. Cambridge University Press, Cambridge, pp 291–348

Wehner R, Müller M (2006) The significance of direct sunlight and polarized skylight in the ant's celestial system of navigation. Proc Natl Acad Sci 103:12575–12579

Weir PT, Dickinson MH (2012) Flying *Drosophila* orient to sky polarization. Curr Biol 22:21–27

Wendt B, Homberg U (1992) Immunocytochemistry of dopamine in the brain of the locust *Schistocerca gregaria*. J Comp Neurol 321:387–403

Wernet MF, Desplan C (2004) Building a retinal mosaic: cell-fate decision in the fly eye. Trends Cell Biol 14:576–584

Wernet MF, Velez MM, Clark DA, Baumann-Klausener F, Brown JR, Klovstad M, Labhart T, Clandinin TR (2012) Genetic dissection reveals two separate retinal substrates for polarization vision in *Drosophila*. Curr Biol 22:12–20

White RH, Xu H, Münch TA, Bennett RR, Grable EA (2003) The retina of *Manduca sexta*: rhodopsin expression, the mosaic of green-, blue- and UV-sensitive photoreceptors, and regional specialization. J Exp Biol 206:3337–3348

Williams DS (1983) Changes of photoreceptor performance associated with the daily turnover of photoreceptor membrane in locusts. J Comp Physiol 150:509–519

Wilson M, Garrard P, McGinness S (1978) The unit structure of the locust compound eye. Cell Tissue Res 195:205–226

Wolburg-Buchholz K (1979) The organization of the lamina ganglionaris of the hemipteran insects, *Notonecta glauca*, *Corixa punctata* and *Gerris lacustris*. Cell Tissue Res 197:39–59

Zufall F (1984) Physiologische und morphologische Charakterisierung der Retinalazellen im Komplexauge der Grillen (*Gryllus bimaculatus*). Diploma thesis, Freie Universität Berlin

Zufall F, Schmitt M, Menzel R (1989) Spectral and polarized light sensitivity of photoreceptors in the compound eye of the cricket (*Gryllus bimaculatus*). J Comp Physiol A 164:597–608